Glycosaminoglycan Disaccharide Alters the Dimer Dissociation Constant of the Chemokine MIP-1β[†]

Melissa A. McCornack, Danielle M. Boren, and Patricia J. LiWang*

Department of Biochemistry and Biophysics, Texas A&M University, TAMU 2128, College Station, Texas 77843-2128

Received February 3, 2004; Revised Manuscript Received May 11, 2004

ABSTRACT: Chemokines are immune system proteins that recruit and activate leukocytes to sites of infection. This recruitment is believed to involve the establishment of a chemokine concentration gradient by the binding of chemokines to glycosaminoglycans (GAGs). In previous studies, we elucidated the GAG binding site of the chemokine MIP-1β and implicated the involvement of the chemokine dimer in GAG binding through residues across the dimer interface. In the present studies, nuclear magnetic resonance spectroscopy was used to investigate the effect of GAG binding on MIP-1β dimerization. Using several dimerization-impaired variants of MIP-1β (F13Y, F13L, L34W, and L34K), these studies indicate that the addition of disaccharide to the mutants increases their dimerization affinities. For MIP-1β F13Y, the presence of the disaccharide increases the chemokine dimerization affinity about 9-fold as evidenced by a decrease in the dimer dissociation constant from 610 to 66 μM. Even more dramatically, the dimerization affinity of MIP-1β L34W also increases upon addition of disaccharide, with the dimer dissociation constant decreasing from 97 to 6.5 μM. After this effect for the mutants of MIP-1β was shown, similar experiments were conducted with the CC chemokine RANTES, and it was demonstrated that the presence of disaccharide increases its dimerization affinity by almost 7-fold. These findings provide further evidence of the importance of the dimer in chemokine function and provide the first quantitative investigation of the role of GAGs in the manipulation of the MIP-1β quaternary structure.

Chemotactic cytokines (chemokines) are a superfamily of small structurally related immune system proteins that play key roles in the immune and inflammatory responses, primarily by recruiting and activating various types of immune system cells (*1*). Traditionally, chemokines have been divided into four subfamilies (CC, CXC, CX_3C, and C), on the basis of the positioning of conserved cysteine residues at their N termini, with the CC and CXC being the largest subfamilies. Chemokine signaling is largely mediated by the binding of these proteins to members of a subclass of seven-transmembrane G-protein-coupled receptors. For three CC chemokines, MIP-1β,[1] MIP-1α, and RANTES, interaction with the CC chemokine receptor CCR5 is not only vital for chemotaxis and leukocyte activation, but also results in these proteins being inhibitory toward certain types of HIV-1 infection. Studies have shown that "R-5 strains" of HIV-1 use CCR5 as a coreceptor, making contacts with the chemokine receptor that are essential for entry into host cells. As a result, MIP-1β, MIP-1α, and RANTES, the natural ligands of CCR5, have been shown to effectively inhibit "R-5" HIV-1 infection primarily by blocking the receptor but also by internalization and down regulation of CCR5 consequent to chemokine receptor interaction (as reviewed in ref *2*).

In addition to their cognate receptors, chemokines interact with glycosaminoglycans (GAGs), anionic polysaccharides located on the endothelial surface and the extracellular matrix. Evidence suggests that the interaction of chemokines with GAGs such as heparan sulfate plays an important role in their biological activity, likely involved in the formation of chemokine gradients necessary for chemotaxis (*3*−*5*). Importantly, although studies demonstrate that mutation of residues in the GAG binding sites of several chemokines including MIP-1β still allow in vitro chemotactic activity, the mutant proteins are unable to recruit cells in vivo (*6*, *7*). This suggests that interaction with GAGs is necessary to establish the requisite chemokine gradient for in vivo chemotaxis.

A variety of techniques including NMR, mutagenesis, and modeling have been used to analyze the GAG binding sites of several chemokines, so that data have been gathered for CC chemokines such as MIP-1β (*8*−*10*), MIP-1α (*11*−*13*), RANTES (*14*−*16*), and MCP-1 (*6*, *17*) and for the CXC chemokines IL-8 (*18*), PF-4 (*19*), SDF-1α (*20*, *21*), and CXCL10 (*22*). These studies have shown that the interaction of chemokines with GAGs is largely electrostatic in nature,

[†] Funding was provided by the National Institutes of Health 1R01AI/HL47832 and by the Robert Welch Foundation A1472.

* To whom correspondence should be addressed: Department of Biochemistry and Biophysics, Texas A&M University, TAMU 2128, College Station, TX 77843-2128. E-mail: pliwang@tamu.edu. Telephone: (979) 845-5616. Fax: (979) 845-9274.

[1] Abbreviations: CCR, CC chemokine receptor; DSS, 2,2-dimethyl-2-silapentane-5-sulfonic acid; GAG, glycosaminoglycan; HIV, human immunodeficiency virus; HSQC, heteronuclear single-quantum coherence; IL-8, interleukin-8 (also referred to as CXC chemokine ligand 8 or CXCL8); K_d, dissociation constant; MCP-1, monocyte chemotactic protein, CCL2; MIP, macrophage inflammatory protein (MIP-1β, CCL4; MIP-1α, CCL3); NMR, nuclear magnetic resonance; PF-4, platelet factor 4 (CXCL4); RANTES, regulated on activation of normal T cell expressed and secreted (CCL5); SDF-1α, stromal cell-derived factor 1α (CXCL12); τ_c, molecular correlation time; T_2, transverse relaxation time constant.

10.1021/bi049751u CCC: $27.50
Published on Web 07/15/2004

involving positively charged residues on the protein surface in ionic interactions with the polyanionic GAGs, with greater affinity for the more highly sulfated GAGs (*23*).

Within the chemokine superfamily and even inside its subclasses, differences exist in the residues involved in GAG binding. Many of the CXC chemokines, such as IL-8, utilize basic residues located in their C-terminal α helices (*18*, *19*), although SDF-1α makes use of basic residues in its first β strand (*20*, *21*). CC chemokines such as MIP-1β, MIP-1α, and RANTES most commonly use basic residues in their 40's region (*8*−*12*, *14*−*16*). For example, the simultaneous mutation of all three positively charged residues in this region of MIP-1β (K45A/R46A/K48A) totally abolishes heparin-binding ability, as judged by heparin affinity chromatography (*8*). Investigating the GAG binding properties of chemokines is complicated by the propensity of chemokines to form high-order aggregates in the presence of GAGs. Chemokines aggregate and sometimes precipitate in the presence of tetra- and larger oligosaccharides (refs *24*, *25*, McCornack and LiWang, unpublished). To overcome this obstacle, disaccharides, although likely too short to provide the full range of chemokine interactions, are often used to investigate structural properties of the GAG−chemokine interaction (*10*, *14*, *18*).

Structural studies of unliganded chemokines show that many form tight dimers, including the CC chemokines MIP-1β, MIP-1α, and RANTES, each forming dimers under acidic conditions and higher order aggregates at near neutral pH (*26*−*30*). Figure 1A shows the residues of wild type MIP-1β that we have shown to be involved in binding heparin disaccharides mapped onto the dimeric structure of the chemokine (*10*, *26*). It has been unclear if the chemokine dimer has any physiological significance, because studies demonstrated that monomeric variants of MIP-1β and other chemokines efficiently bind and activate their cognate receptors in vitro (*31*−*33*). However, recently it has been reported that both the ability to form dimers and to interact with GAGs were necessary for in vivo activity for some chemokines, including MIP-1β, RANTES, and MCP-1 (*6*). Although the chemokine dimer does not appear to be involved in the receptor function, it is possible that the dimer may instead be an important mediator of GAG binding. Our previous studies suggested this might be the case, because it was found that residues Met3, Gly4, and Ser5 are involved in the binding of disaccharide to dimeric MIP-1β across the dimer interface (Figure 1A), possibly completing the GAG binding pocket. In accordance with this, the data also showed that dimeric MIP-1β binds disaccharide with higher affinity than does a monomeric MIP-1β variant (*10*).

To investigate the interrelationship of GAG binding and chemokine quaternary structure, the present study used mutagenesis techniques and NMR methodologies to determine the possible role of GAGs in the dimerization of the chemokine MIP-1β. Because of the tight dimer dissociation constant of wild type MIP-1β [dimer $K_d = 0.73\ \mu M$, in the presence of 150 mM NaCl (*31*)], it was not feasible to use this protein in quantitative NMR studies, which rely upon the direct visualization of resonances from both the dimeric and monomeric forms. Therefore, we studied several mutants of MIP-1β having weakened dimerization affinities and showed that in each case, where a dimer K_d was measured,

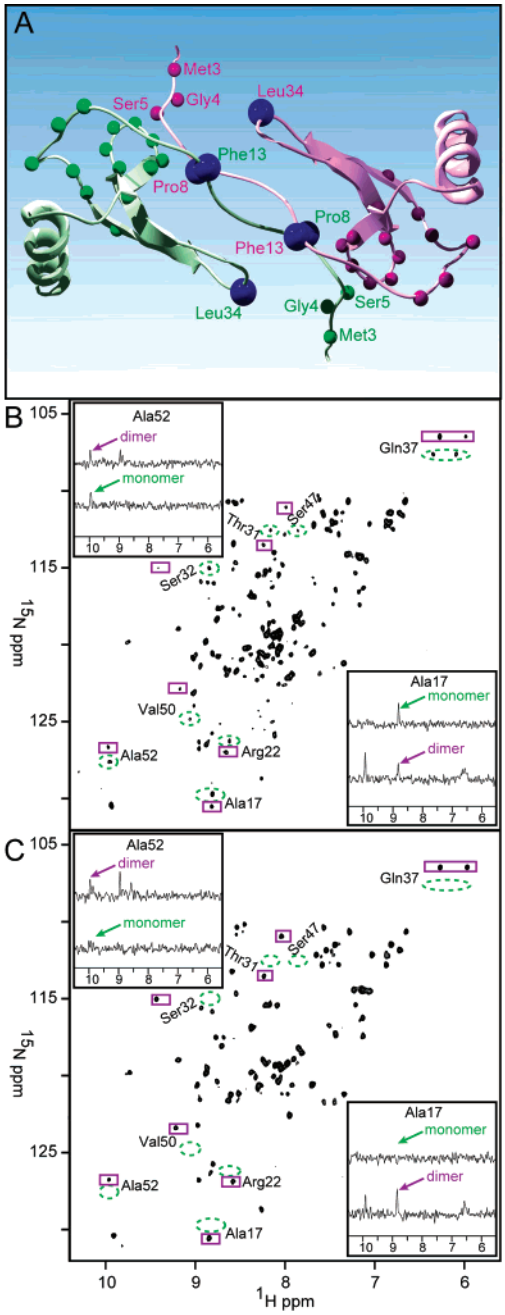

FIGURE 1: Wild type MIP-1β. (A) Ribbon diagram of the homodimer of the CC chemokine MIP-1β [PDB accession number 1hum (*26*)]. Large blue spheres represent the backbone amide nitrogen atoms of several residues of wild type MIP-1β known to be important for dimerization (*31*) and that are mutated in the present study. Small green and purple spheres represent residues reported to be affected upon disaccharide binding (*10*), where the green spheres represent residues from the light green subunit and the purple spheres, the light purple subunit. The ^{1}H-^{15}N HSQC spectra for (B) 0.01 mM MIP-1β wild type in the absence of heparin disaccharide and (C) 0.01 mM MIP-1β wild type in the presence of 0.5 mM heparin disaccharide I-P. The resonances from select residues that display both dimer and monomer peaks are enclosed in purple boxes and green dashed ovals, respectively (*26*, *34*, *42*). The upper left inserts in B and C show the one-dimensional traces in the ^{1}H dimension for the dimer and monomer resonances of the Ala52 residue. Likewise, the lower right inserts show the one-dimensional traces in the ^{1}H dimension for the dimer and monomer resonances of the Ala17 residue. In these inserts, arrows are used to indicate the peak positions for either Ala52 or Ala17, with purple arrows for the dimer resonances and green arrows for the monomer resonances.

the presence of heparin disaccharide tightens the chemokine dimer by greater than 6-fold. Furthermore, this effect is also seen in the wild type CC chemokine RANTES.

EXPERIMENTAL PROCEDURES

Materials. The disulfated heparin disaccharide I-P (2-aminocarboxyethyl-2-deoxy-3-*O*-(2-*O*-sulfo-β-D-gluco-4-enepyranosyluronic acid)-6-*O*-sulfo-D-glucosamine, trisodium salt) was obtained from both Calbiochem−Novabiochem Corp. (La Jolla, CA) and Sigma−Aldrich Co. (St. Louis, MO) and used without further purification. $^{15}NH_4Cl$ and ^2H_2O were purchased from Spectra Gases Inc. (Columbia, MD) and Martek Biosciences Corp. (Columbia, MD), respectively. The recombinant proteases, factor Xa and enterokinase, were obtained from Novagen (Madison, WI).

Stock solutions of heparin disaccharide I-P (20 mM) were prepared by dissolving the purchased aliquots in either H_2O or ^2H_2O and kept frozen until use. The concentration of each I-P stock solution was determined based on the amount specified by the commercial suppliers. Each respective commercial source was contacted as to the magnitude of possible error in the quantity purchased; the error in disaccharide I-P obtained from Calbiochem−Novabiochem Corp. was ±1.0%, and the amount provided by Sigma−Aldrich Co. may exceed the specified quantity by a maximum of 20%.

The plasmids containing the sequences coding for the mature forms of rhesus macaque MIP-1α and RANTES were obtained by isolation from cell stocks received from the NIH AIDS Research and Reference Reagent Program, Division of AIDS, National Institute of Allergy and Infectious Diseases. For both MIP-1α and RANTES, the chemokine gene was located in the *Kpn*I−*Bam*HI site of pET32a vector (Novagen, Madison, WI). The rhesus macaque MIP-1α gene was sequenced and found to code an amino acid sequence identical to that of its respective human sequence (accession number AAC03539), with an additional N-terminal Phe-Ser. Likewise, the amino acid sequence of the mature rhesus macaque RANTES gene was identical to the amino acid sequence of human RANTES used for structure determination [PDB accession number 1rtn (*27*)].

Protein Preparation. Wild type MIP-1β and its dimer-impaired variants F13Y, F13L, F13W, L34W, L34K, P8I, and P8V were expressed using a modified pET32LIC vector (Novagen, Madison, WI) lacking the thioredoxin portion of the fusion tag. Construction of the vector constructs containing the F13W, L34W, L34K, P8I, and P8V mutants of MIP-1β was achieved by standard thermocycling polymerase reaction procedures as was reported earlier for the constructs of the MIP-1β mutants F13Y and F13L (*31*). Sequencing of the genes to confirm the mutations was carried out using standard methods.

For protein expression, the modified pET32LIC vectors containing the genes for the MIP-1β mutants and the pET32a vectors containing the MIP-1α and RANTES genes were transformed into competent BL21(DE3) cells (Novagen, Madison, WI). ^{15}N-labeled proteins were expressed and then purified from inclusion bodies by a procedure modified from that reported previously (*34*). In the adapted purification procedure, the refolded proteins were dialyzed against 2 × 2 L of 20 mM Tris at pH 8.0 containing 50 mM NaCl, followed by purification using C4 reversed-phase chromatography and lyophilization. The fusion tags were then proteolytically cleaved using either recombinant factor Xa for the MIP-1β variants or recombinant enterokinase for MIP-1α and RANTES. The cleaved proteins were then purified using C4 reversed-phase chromatography and lyophilized. NMR samples were prepared by dissolving lyophilized protein in a standard buffer of 20 mM sodium phosphate (pH 2.8) containing 10% ^2H_2O and 0.02% sodium azide. Protein concentrations were determined by measuring the absorbance at 280 nm and using extinction coefficients calculated with tools on the ExPASy web server (*35*). The extinction coefficients are as follows: wild type MIP-1β, MIP-1β F13L, MIP-1β L34K, MIP-1β P8I, MIP-1β P8V, and RANTES, 12 330 cm^{-1} M^{-1}; MIP-1β F13Y, 13 610 cm^{-1} M^{-1}; MIP-1β L34W and MIP-1β F13W, 18 020 cm^{-1} M^{-1}; and MIP-1α, 9770 cm^{-1} M^{-1}. Mass spectral analysis was performed on the purified RANTES and a *m*/*z* ratio of 7860 was found, which was in good agreement with the expected molecular weight of 7947 g/mol for the uniformly ^{15}N-labeled protein.

Analytical Ultracentrifugation. Sedimentation equilibrium experiments were performed on a Beckman XL-A analytical ultracentrifuge equipped with absorbance optics. Data were collected at 26 500, 37 400, 45 900, 53 000, and 60 000 rpm at 25 °C for samples of MIP-1β F13Y in 20 mM sodium phosphate at pH 2.8. Centrifugation experiments were monitored at 280 nm on samples having protein concentrations of 18, 31, and 43 μM. Data editing and analysis were performed using UltraScan version 6.0 (*36*).

NMR Spectroscopy. All NMR spectra were acquired at 25 °C on either a 500 or 600 MHz Varian Inova spectrometer and then processed and analyzed using NMRPipe (*37*) and PIPP (*38*), respectively. Chemical shifts were referenced relative to DSS (*39*). For wild type MIP-1β, ^{1}H-^{15}N HSQC spectra were measured on the 600 MHz spectrometer with 450* points in the ^{1}H (t_2) dimension and 128* points in the ^{15}N dimension (t_1), where *n** represents *n* complex points. The ^{1}H and ^{15}N spectral widths in these experiments were 7200.720 and 1800.018 Hz, respectively. For all other proteins, ^{1}H-^{15}N HSQC spectra were acquired on the 500 MHz spectrometer with 512*(t_2) × 128*(t_1) points and spectral widths of 6000.6 Hz (^{1}H) and 1500.015 Hz (^{15}N). All data were processed with 90°-shifted squared sine-bell apodization in both t_1 and t_2 followed by zero filling to final digital resolutions of 4.7 Hz/point (F_1) and 5.3 Hz/point (F_2) for the data measured on the 600 MHz spectrometer and 3.9 Hz/point (F_1) and 3.9 Hz/point (F_2) for the data measured on the 500 MHz spectrometer. To confirm the resonance assignments of RANTES, an HNHA experiment (*40*) was measured on a 1.5 mM RANTES sample and used in conjunction with the published chemical shift assignments (*27*, *30*).

Addition of Disaccharides to MIP-1β Variants and RANTES. To initially ascertain the effect that the presence of disaccharide had upon the monomer−dimer equilibrium of MIP-1β, ^{1}H-^{15}N HSQC spectra were measured on dilute samples of wild type MIP-1β (0.010 mM) in the absence of heparin disaccharide and in the presence of 0.5 mM disaccharide I-P. Qualitatively, the relative intensities of select monomer and dimer resonances of the protein were monitored so as to judge the amount of each species in solution. Similarly,

heparin disaccharide I-P (from 0 to as much as 3 molar equiv) was added to the dimer-impaired MIP-1β variants F13Y, F13L, F13W, L34W, and L34K. Using a 20 mM stock solution, increasing amounts of disaccharide I-P were added to samples of 0.19−0.25 mM ^{15}N-labeled mutant protein; ^{1}H-^{15}N HSQC spectra were acquired for each addition; and the relative intensities of monomer and dimer resonances were monitored. Finally, heparin disaccharide I-P (from 0 to 2 molar equiv) was added to RANTES (0.059 mM); ^{1}H-^{15}N HSQC spectra were acquired; and the relative amounts of monomeric and dimeric RANTES were monitored.

Quantitation of the Change in Dimerization Affinity of the MIP-1β Variants and RANTES. To quantify the effect of disaccharide on the dimer K_d of MIP-1β, dilution experiments were conducted in the absence of heparin and in the presence of a constant, saturating amount of heparin disaccharide I-P for the dimer-impaired mutants MIP-1β F13Y and MIP-1β L34W. In the absence of disaccharide, ^{1}H-^{15}N HSQC spectra were acquired for the F13Y variant at various dilutions from 1.5 to 0.059 mM protein. In the presence of 1 mM disaccharide I-P, spectra of MIP-1β F13Y were measured at dilutions from 0.43 to 0.018 mM protein. For the L34W variant, ^{1}H-^{15}N HSQC spectra were acquired at dilutions from 0.47 to 0.040 mM in the absence of disaccharide and from 0.26 to 0.019 mM in the presence of 0.5 mM disaccharide I-P. For wild type RANTES, dilution experiments were conducted from 1.2 to 0.025 mM protein in the absence of disaccharide. In the presence of 0.5 mM heparin disaccharide I-P, spectra of 0.018 and 0.040 mM RANTES were measured. In all ^{1}H-^{15}N HSQC experiments, signal averaging was drastically increased for the more dilute samples such that the signal-to-noise ratio of the less-populated quaternary form was 2:1 or greater, resulting in data of sufficient quality for analysis.

In the case of a simple monomer−dimer equilibrium $M + M \leftrightarrow D$, the fractional population of the total polypeptide subunits in the dimer state Θ_d and the dimer K_d are related as

$$K_d = [M][M]/[D] = (C_o - C_o\Theta_d)^2/(0.5C_o\Theta_d) \quad (1)$$

where C_o is the total concentration of polypeptide subunits ($C_o = [M] + 2[D]$), $[M]$ is the concentration of monomer, and $[D]$ is the concentration of dimer. Rearrangement of this equation gives Θ_d in terms of C_o as

$$\Theta_d = (0.5/C_o)\{(2C_o + 0.5K_d) - ((2C_o + 0.5K_d)^2 - 4(C_o)^2)^{1/2}\} \quad (2a)$$

This equation was found to adequately fit the data at lower protein concentrations. However, for the proteins MIP-1β F13Y and L34W in the absence of disaccharide, the fits were increasingly poor at higher protein concentration because of the presence of protein aggregation that manifested as incorrect reporting of Θ_d. To account for this, an additional variable (α) was used in the fitting equation (eq 2b). To be consistant, all K_d values reported were fit with this equation, although the variable α was essentially 1.0 for L34W in the presence of disaccharide and for RANTES. The highest α values determined were 1.2−1.5 for amide residues of F13Y in the absence of disaccharide.

$$\Theta_d/\alpha = (0.5/C_o)\{(2C_o + 0.5K_d) - ((2C_o + 0.5K_d)^2 - 4(C_o)^2)^{1/2}\} \quad (2b)$$

Although the total protein concentration, C_o, can be measured directly using an absorbance at 280 nm, the separate concentrations of monomer and dimer cannot. Instead, the relative intensities of monomer and dimer resonances in an NMR spectrum (here, the ^{1}H-^{15}N HSQC spectrum) can be used in the determination of Θ_d. The observed intensities of the monomer (I_m) and dimer (I_d) resonances are proportional to the fractional population of polypeptide subunits contributing to each state. In other words, I_m is proportional to $[M]/C_o$ ($\equiv \Theta_m$) and I_d, to $2[D]/C_o$ ($\equiv \Theta_d$). In the calculation of Θ_d using the intensities of NMR resonances, the difference in molecular correlation time (τ_c) between the monomer and dimer must be considered. For a Lorentzian peak at resonance, the signal intensity is proportional to the transverse relaxation time constant T_2 and the line width at half-height is given as $(\pi T_2)^{-1}$ in hertz (*41*). Because of its larger size, the dimeric species has a larger τ_c than that of the monomeric species. Because T_2 itself is proportional to $(\tau_c)^{-1}$ (*41*), a larger τ_c corresponds to a shorter T_2 value for the dimer, a broader line width for the dimer, and an apparent decrease in I_d, when compared to I_m for equal amounts of polypeptide subunits. Therefore, the relative intensity of a dimer resonance was multiplied by the ratio $\tau_{c,dimer}/\tau_{c,monomer}$ to meaningfully compare I_d and I_m. When the difference in τ_c is compensated for, Θ_d is related to I_d as follows, where $I_{d,corrected}$ is the corrected intensity of the dimer resonance

$$\Theta_d = I_{d,corrected}/(I_{d,corrected} + I_m) \quad (3)$$

In the dilution experiments of the MIP-1β variants F13Y and L34W and for those of wild type RANTES, the intensities of nondegenerate monomer (I_m) and dimer (I_d) HSQC resonances for select residues (see the Results for the residues used) were monitored at each point in the dilution series both in the absence and presence of disaccharide I-P. Because the MIP-1β variants and RANTES have essentially the same molecular mass, the correction of I_d for the difference in τ_c of the dimer as compared to the monomer was accomplished using the published τ_c values for MIP-1β; to our knowledge, no values have been published for RANTES. Values of τ_c reported previously for the monomeric MIP-1β F13A variant (5.52 ns) and the dimeric wild type MIP-1β (8.07 ns) were used (*42*). For each dilution series, Θ_d was plotted versus C_o and the data were fit to eq 2b using KaleidaGraph 3.5 (Synergy Software, Reading, PA) to yield a dimer K_d for each of the select residues investigated. The individual K_d values were then averaged to report an overall dimer K_d value for each protein either in the absence or presence of heparin disaccharide I-P. Error in Θ_d for each data point was estimated from the signal-to-noise ratio of the corresponding NMR spectrum and was used to weight the curve fitting (*43*). Because of the relatively tight RANTES dimer in the presence of heparin disaccharide I-P, only two concentration points were measured (0.018 and 0.040 mM RANTES, both in the presence of 0.5 mM I-P) rather than a full dilution curve. Approximate dimer K_d values were then estimated from the data at each of these RANTES concentrations in the following manner. First, from the NMR

data, Θ_d values were calculated for each of the select residues (H23, K25, T30, and S64) using eq 3. These Θ_d values were then input into eq 1, obtaining a dimer K_d value for each residue at each concentration. Finally, the individual residue K_d values at each RANTES concentration point were averaged. Although not as accurate as a full curve, this method was employed because the very dilute concentrations needed to define a full binding curve were not amenable to NMR.

As a control for the effect that ionic strength changes occurring with disaccharide addition have upon MIP-1β dimerization affinity, NaCl was added to a 0.26 mM MIP-1β F13Y sample at 0, 4, and 10 molar equiv (0, 1.0, and 2.6 mM) and the resulting HSQC spectra were measured. The average dimer K_d of MIP-1β F13Y at each salt concentration was calculated using the single point method described above for RANTES in the presence of disaccharide I-P.

RESULTS

Analytical Ultracentrifugation. To quantify the effect of heparin disaccharide on the dimerization of MIP-1β, analytical ultracentrifugation was attempted on the dimer-impaired MIP-1β variant F13Y. This technique generally requires the presence of salt (0.1−0.2 M) in the buffer to suppress thermodynamic nonideality arising from charge−charge repulsion between solutes (*44*, *45*). However, these levels of salt abolish the ability of the chemokine to bind heparin disaccharides (data not shown). Analytical ultracentrifugation was attempted in the absence of salt, resulting in nonideal curves that could not be fit. Therefore, these experiments were discontinued in favor of NMR methods.

Dimer-Impaired MIP-1β Mutants. To study the effect of disaccharide binding upon the dimerization of the CC chemokine MIP-1β, a strategy combining mutagenesis and structural analysis using ^{1}H-^{15}N HSQC NMR experiments was pursued. In the ^{1}H-^{15}N HSQC experiment, each directly bonded N−H pair in the protein gives rise to a resonance, the position of which is sensitive to changes in the environment about those nuclei. As a result, the spectrum is highly sensitive to changes in secondary, tertiary, and quaternary structure and also provides evidence that a protein is folded upon mutation. Because the ^{1}H-^{15}N HSQC spectra for both dimeric and monomeric MIP-1β variants have been sequentially assigned and have been shown to exhibit characteristic resonance patterns resulting from their different quaternary structures (*26*, *34*, *42*), this experiment allows for a relatively quick assessment of the effect of the point mutation upon the dimerization of MIP-1β.

Ideally, a study to determine the effect of heparin upon dimerization affinity of MIP-1β would involve investigation of the wild type protein. An accurate estimate of the dimer K_d of a protein by NMR requires a series of spectra at different protein concentrations each providing information on the amounts of both dimer and monomer in solution. At dilute NMR conditions (0.01 mM) requiring significant signal averaging (2 days), weak resonances for both dimer (enclosed in purple squares) and monomer (green dashed ovals) are observable in the ^{1}H-^{15}N HSQC spectrum of wild type MIP-1β (Figure 1B), characteristic of an equilibrium between the quaternary species with slow exchange on the NMR time scale. However, measuring a series of such spectra at around this concentration with sufficient signal-to-noise to calculate a dimer K_d is not feasible. Qualitatively, the relative intensities of the dimer and monomer resonances in this spectrum of wild type MIP-1β suggests a dimer K_d of approximately 5 μM in the absence of any NaCl. As expected for a hydrophobic dimer interface, this is significantly weaker than that determined previously in the presence of NaCl (*31*). Upon addition of disaccharide, the monomer peaks are no longer observable above the noise of the spectrum (Figure 1C) suggesting that the addition of heparin disaccharide significantly alters the equilibrium, favoring the dimer.

To more accurately quantify the effect of the binding of disaccharide I-P upon MIP-1β dimerization, mutants of the chemokine with weakened dimer affinities were designed so that entire dilution curves could be obtained at protein concentrations amenable to NMR studies. These mutations were made at different locations on the protein, each distal from the heparin binding site (Figure 1A). As our previous studies have shown, point mutations of MIP-1β at the residues Pro8, Phe13, and Leu34 result in folded variants whose affinities for dimerization are weakened to varying degrees (*31*). In addition to the MIP-1β F13Y and F13L mutants reported earlier (*31*), the following mutants of MIP-1β were constructed and investigated: F13W, P8I, P8V, L34W, and L34K. The ^{1}H-^{15}N HSQC spectra of each of these proteins (0.19−0.25 mM) indicated that all were folded (data not shown). Whereas the F13W, P8V, and P8I mutants were purely monomeric at the concentrations investigated (data not shown), the F13Y, F13L, L34W, and L34K variants exhibited both monomer and dimer resonances, characteristic of an equilibrium between the quaternary species. Our previous results indicated that purely monomeric variants such as MIP-1β P8A and the truncation mutant MIP(9) do not show a tendency to dimerize in the presence of disaccharide (*10*). Similarly, in the present study, the quaternary state of purely monomeric F13W mutant was found to be unaffected by the addition of disaccharide I-P. Therefore, this mutant and the purely monomeric P8I and P8V variants were not studied further. To probe the effect that heparin disaccharide binding has on the dimerization affinity of the dimer-impaired MIP-1β variants, experiments on mutants of MIP-1β at residue positions Phe13 and Leu34 were then investigated in turn.

Effect of Disaccharide Binding on the Dimerization of the Phe13 Mutants. To ascertain whether the presence of disaccharide would alter the dimerization of the Phe13 variants of MIP-1β, increasing amounts of heparin disaccharide I-P were added to the F13Y and F13L variants. Parts A and B of Figure 2 show a part of the two-dimensional ^{1}H-^{15}N HSQC spectrum containing the monomer and dimer resonances of Ala52 for the F13Y variant in the absence and presence of disaccharide, respectively. To the right of each spectrum is a one-dimensional trace through each resonance along the ^{1}H dimension. In this F13Y variant (0.24 mM), the traces clearly show that the intensity of the dimer resonance is approximately one-half that of the monomer in the absence of disaccharide (Figure 2A). Upon addition of disaccharide (0.75 mM) to the protein, the intensity of the dimer resonance is seen to be significantly greater than that of the monomer (Figure 2B). Analogous results were observed for the F13L variant (data not shown). These results indicate that, like the wild type protein, for the dimer-

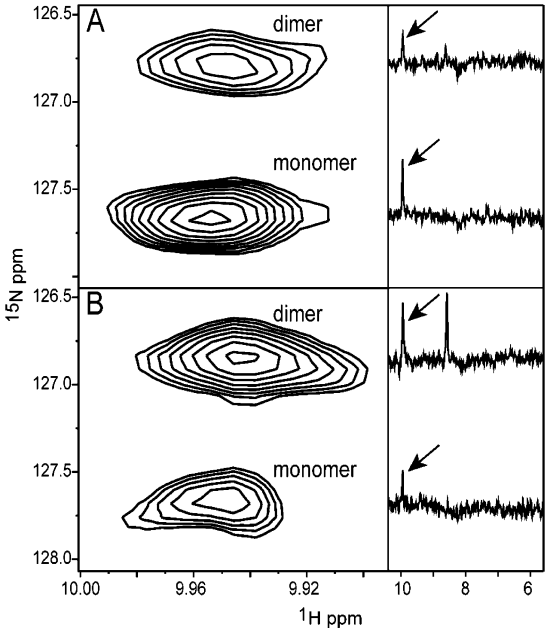

FIGURE 2: Addition of heparin disaccharide I-P to MIP-1β F13Y. In the left-hand panels, the Ala52 region of the ^{1}H-^{15}N HSQC spectra for (A) 0.24 mM MIP-1β F13Y in the absence of disaccharide and (B) 0.24 mM MIP-1β F13Y in the presence of 0.75 mM disaccharide I-P is shown. In the right-hand panels, one-dimensional traces in the ^{1}H dimension for these resonances are shown, where an arrow is used to indicate the corresponding peak position.

impaired MIP-1β mutants at the Phe13 position, the presence of disaccharide causes a shift in the monomer−dimer equilibrium favoring dimerization.

To quantify the increased dimerization affinity of MIP-1β F13Y in the presence of heparin disaccharide I-P, dilution experiments were conducted on the protein both in the absence of heparin and in the presence of a constant, saturating amount of disaccharide. In the absence of disaccharide, changes in the resonance intensities of select residues having easily identifiable, resolved dimer and monomer resonances in the ^{1}H-^{15}N HSQC spectra were monitored during the dilution of the protein from 1.5 to 0.059 mM. These were the backbone amide resonances of C12, A17, R22, V25, T31, S32, C35, R46, S47, K48, V50, and A52 and the side chain amide resonances of Q37. Characteristic of a dissociation event with slow exchange between the different quaternary forms on the NMR time scale, the dimeric species predominated at the higher concentrations, whereas the more dilute concentrations favored the monomer. Parts A−C of Figure 3 (—, ●) show the curves obtained for residues Ala52, Ser32, and Arg22 in the serial dilution of the F13Y variant in the absence of disaccharide. The fractional population of total subunits in the dimer state, Θ_d, was plotted versus the total polypeptide concentration, C_o, and subsequently fit using eq 2b. Similar curves were also plotted and fit for the other residues mentioned previously. As described in Experimental Procedures, the high concentrations of MIP-1β F13Y that were necessary to complete this curve required an additional fitting parameter to account for possible aggregation that resulted in error in Θ_d. In the worst case (MIP-1β F13Y in the absence of disaccharide), this parameter was found to range from 1.2−1.5. The dimer K_d obtained by averaging the values calculated for each of the individual residues was found to be 580 ± 140 μM (Table 1). Because the effects of exchange and disaccharide binding upon signal intensity were unknown, the average dimer K_d was then recalculated with the elimination of the data from the side chain of Q37 and the data from residues known to be directly involved in GAG binding (V25, R22, R46, S47, K48, and V50) (*8*, *10*). With this smaller subset of residues, the average dimer K_d was determined not to change significantly and to be 610 ± 130 μM. Not unexpectedly, this value differs from that determined previously for this mutant in the presence of 150 mM NaCl [K_d = 43 μM (*31*)] because the MIP-1β dimer has been shown to be strongly affected by solution conditions (*34*).

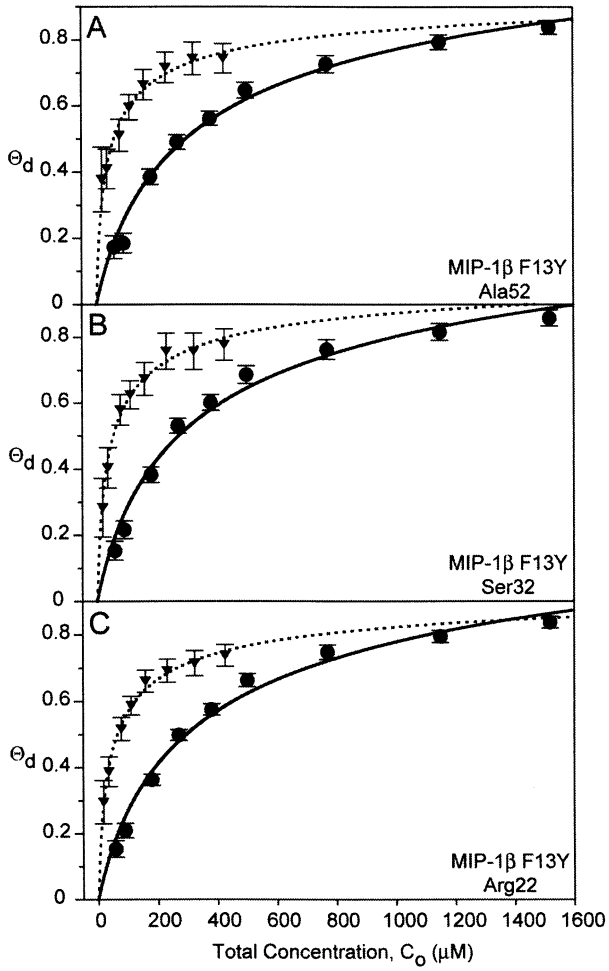

FIGURE 3: Plots of the fractional population of MIP-1β F13Y polypeptide subunits in the dimeric state as a function of the total concentration of subunits in the absence (—, ●) and presence (- - -, ▼) of 1 mM heparin disaccharide I-P. Representative data for residues Ala52 (A), Ser32 (B), and Arg22 (C) are shown. After NMR intensity information obtained in serial dilution experiments is calculated, the fractional population of polypeptide subunits in the dimeric state Θ_d (given by eq 3) is plotted versus the total polypeptide concentration C_o as determined using the absorbance at 280 nm. The data are fit to eq 2b, yielding a dimer dissociation constant K_d. The noise level of each HSQC spectrum is used to calculate the error in Θ_d at each corresponding data point. The resulting error values are shown in the figures and are used in the weighting of each point in the curve fit.

Similar dilution experiments were conducted on the F13Y mutant in the presence of heparin disaccharide I-P in which the concentration of I-P remained constant as the protein was diluted. On the basis of our previous results (*10*), 1 mM heparin disaccharide I-P was used in these experiments to

Table 1: Dimer K_d for the MIP-1β Proteins and Wild Type RANTES in the Absence and Presence of Heparin Disaccharide I-P[a]

protein	dimer K_d absence of disaccharide I-P	dimer K_d presence of disaccharide I-P
MIP-1β F13Y	580 ± 140 μM[b]	57 ± 22 μM[b]
	610 ± 130 μM[c]	66 ± 24 μM[c]
MIP-1β L34W	95 ± 19 μM[b]	6.8 ± 2.0 μM[b]
	97 ± 18 μM[c]	6.5 ± 1.5 μM[c]
wild type RANTES	34 ± 12 μM[b]	4.2 ± 1.4 μM[b,d]
		5.0 ± 1.2 μM[b,d]

[a] Error shown for all of the average dimer K_d values represent one standard deviation of the individual residue K_d values used to calculate the average K_d values reported. [b] Values were calculated by averaging the individual dissociation constants found for each of the residues monitored. For MIP-1β F13Y, the residues used were C12, A17, R22, V25, T31, S32, C35, Q37, R46, S47, K48, V50, and A52. For MIP-1β L34W, the residues used were A17, R22, V25, Y29, T31, S32, Q37, S47, K48, V50, and A52. For RANTES, the residues used were H23, K25, T30, and S64. [c] Values were determined using a smaller subset of data where (1) the side chain data for residue Q37 were removed because the effect of exchange was unknown and (2) the data for resonances involved in the disaccharide-binding site (V25, R22, R46, S47, K48, and V50) were removed because the effect of GAG binding on resonance intensity was unknown. [d] Average approximate dimer K_d was determined at two concentration points rather than a complete dilution curve by first using eq 3 to calculate Θ_d for each residue, then inputting the Θ_d values into eq 1 to calculate a dimer K_d for each residue, and finally averaging the individual K_d values. The upper value was calculated for a 0.018 mM RANTES sample and the lower, for a 0.040 mM RANTES sample, each in the presence of 0.5 mM disaccharide I-P.

ensure saturation with disaccharide. Parts A−C of Figure 3 (- - -, ▼) show the curves obtained for residues Ala52, Ser32, and Arg22 in the serial dilution of MIP-1β F13Y in the presence of 1 mM disaccharide. Just as in the absence of disaccharide, curves were also obtained for the backbone amide resonances of C12, A17, V25, T31, C35, R46, S47, K48, and V50 and the side chain amide resonances of Q37. The curves obtained from these data were seen to fit well and yielded an average dimer K_d of 57 ± 22 μM. As above, the average dimer K_d was recalculated with the elimination of the data from the side chain of Q37 and the data from residues known to be directly involved in GAG binding (V25, R22, R46, S47, K48, and V50) (*8*, *10*). With this smaller set of data, the average dimer K_d (66 ± 24 μM) did not change significantly from the larger set of data and was still approximately 9-fold tighter than the protein in the absence of disaccharide (Table 1).

As a control for the effect of increasing ionic strength with the addition of the polyanionic disaccharides in our dilution studies, MIP-1β F13Y (0.26 mM) was titrated with increasing amounts of NaCl (data not shown). Whether using the large set of residues or the smaller subset (described above), the average dimer K_d of MIP-1β F13Y was found to tighten only about 25% with the addition of up to 2.6 mM NaCl, which represents approximately the maximum number of negative ions found in the dilution series. This increase in dimerization affinity was judged to be insubstantial because not only was it on the order of the error seen for the average dimer K_d values of MIP-1β F13Y (Table 1), but it was also much less than the nearly 9-fold difference in the average dimer K_d seen when adding heparin disaccharide I-P.

Effect of Disaccharide Binding on the Dimerization of the Leu34 Mutants. After a marked increase in the dimerization affinity of the MIP-1β F13Y mutant in the presence of disaccharide was seen and quantified, similar experiments were conducted on MIP-1β variants mutated at the Leu34 residue position, specifically L34W and L34K. As with the Phe13 mutants, heparin disaccharide I-P was added to L34W and L34K to qualitatively determine whether disaccharide affects the dimerization affinity of these mutants. Parts A and B of Figure 4 show the traces through the monomer

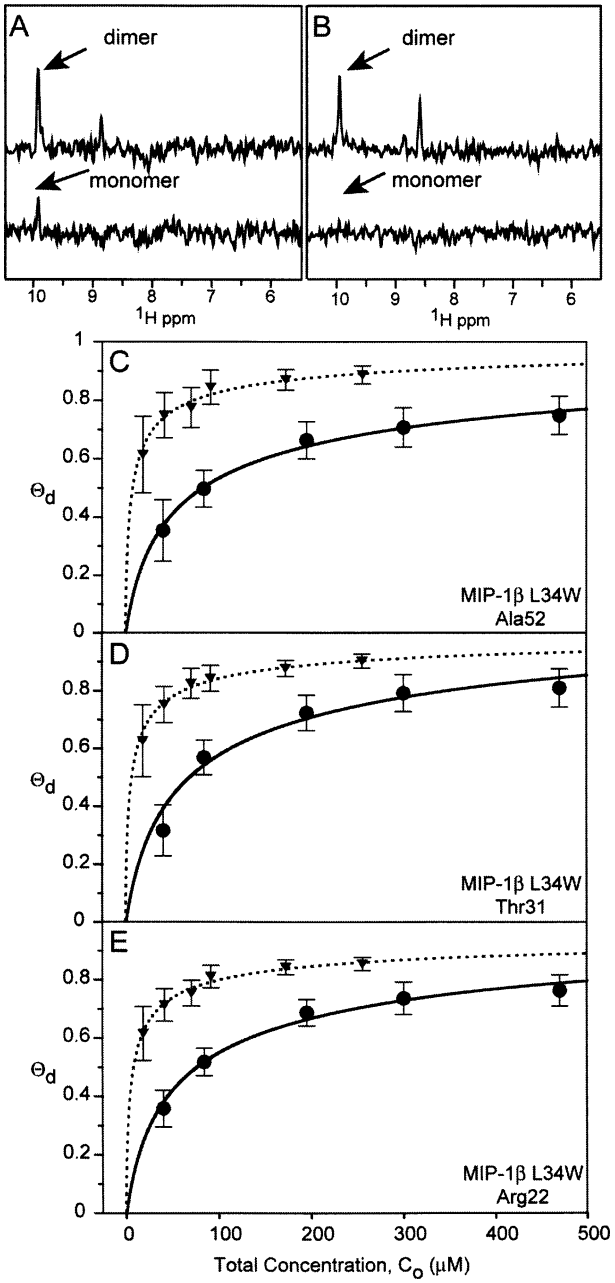

FIGURE 4: Addition of heparin disaccharide I-P to MIP-1β L34W. One-dimensional traces in the ^{1}H dimension of the ^{1}H-^{15}N HSQC spectra through both the dimer and monomer resonances of the Ala52 residue of MIP-1β L34W (0.24 mM) are shown in the absence of heparin (A) and in the presence of 0.75 mM heparin disaccharide I-P (B). The arrows indicate the peak position for Ala52. (C−E) Plots of the Θ_d versus C_o for the dilution series of L34W in the absence of disaccharide (—, ●) and in the presence of disaccharide I-P (- - -, ▼) for residues Ala52, Thr31, and Arg22, respectively. The data are fit to eq 2b, yielding a dimer dissociation constant K_d. The noise level of each HSQC spectrum is used to calculate the error in Θ_d at each corresponding data point. The resulting error values are shown in the figures and are used in the weighting of each point in the curve fit.

and dimer resonances of the section of the ^{1}H-^{15}N HSQC spectrum for the Ala52 residue of the L34W variant in the absence and presence of disaccharide I-P, respectively. In the absence of disaccharide I-P, the spectrum at 0.24 mM protein shows both dimer and monomer resonances (Figure 4A). With the addition of disaccharide I-P to a final concentration of 0.75 mM, the monomer resonance is no longer visible above the noise of the experiment (Figure 4B). Similar results were observed for the L34K variant (data not shown). As was the case for wild type MIP-1β and its Phe13 mutants, these results indicate that the presence of disaccharide causes an increase in the dimerization affinity of the Leu34 mutants of the CC chemokine.

To quantify the increased dimerization affinity suggested by these experiments, serial dilution studies were conducted on the MIP-1β L34W variant both in the absence and presence of heparin disaccharide I-P. The L34W variant was chosen for these experiments over the L34K mutant because it was unclear whether a positively charged Lys residue at position 34 [although not located in the disaccharide binding site (*10*)] would alter the sugar binding affinity. Therefore, for MIP-1β L34W, changes in the monomer and dimer resonance intensities of select residues in the ^{1}H-^{15}N HSQC spectra were monitored during the dilution of the protein from 0.47 to 0.040 mM. Dilution experiments were also conducted in the presence of 0.5 mM heparin disaccharide I-P on MIP-1β L34W from 0.26 to 0.019 mM protein. Parts C−E of Figure 4 show the plots obtained for residues Ala52, Thr31, and Arg22 of MIP-1β L34W when plotting Θ_d versus C_o in the absence (—, ●) and presence (- - -, ▼) of disaccharide I-P. For this protein, data and corresponding curves were obtained for the backbone amide resonances of A17, R22, V25, Y29, T31, S32, S47, K48, V50, and A52 and the side chain amide resonances of Q37. The data sets were fit using eq 2b, yielding average dimer K_d values of 95 ± 19 μM in the absence of I-P and 6.8 ± 2.0 μM in the presence of I-P. As for the F13Y variant, the average values for MIP-1β L34W were recalculated with the elimination of the data from the side chain of Q37 and the data from residues known to be directly involved in GAG binding (V25, R22, S47, K48, and V50) (*8*, *10*) and found to be 97 ± 18 μM (without I-P) and 6.5 ± 1.5 μM (with I-P). Even more substantial than for MIP-1β F13Y, these results show that the disaccharide increases the dimerization affinity of MIP-1β L34W nearly 15-fold.

Other CCR5-Binding Chemokines. Because our findings indicated that the presence of disaccharide alters the dimer dissociation equilibrium of MIP-1β, studies were then conducted to determine whether a similar effect could be generalized to the other CCR5-binding, anti-HIV CC chemokines MIP-1α and RANTES. To ascertain whether the types of experiments conducted for MIP-1β might be used for MIP-1α and RANTES, preliminary dilution experiments were conducted on each protein. In the case of MIP-1α, the protein was diluted from 0.15 to 0.010 mM and ^{1}H-^{15}N HSQC spectra were acquired at each concentration (data not shown). Because there was no doubling, shifting, or appearance/disappearance of resonances, the spectra indicated that under the conditions used, the quaternary state of MIP-1α remained unchanged. Therefore, the NMR dilution experiments described above could not be used with MIP-1α. On the other hand, the preliminary dilution experiments on RANTES (0.57−0.062 mM) suggested behavior indicative of a monomer−dimer equilibrium in slow exchange on the NMR time scale, which was expected based on previously published studies (*27*). For RANTES, assignments of the dimer residues were based on the published chemical shifts (*27*, *30*) and on an HNHA NMR experiment measured for confirmation. New resonances that appeared at low concentration were presumed to arise from the monomeric species. This assumption is supported by the consistently good quality curves obtained in the subsequent dilution studies.

To ascertain whether the presence of disaccharide would alter the dimerization affinity of RANTES, heparin disaccharide I-P was added to the protein. As had been observed for the wild type and the Phe13 and Leu34 variants of MIP-1β, these preliminary experiments with RANTES suggested a shift in the monomer−dimer equilibrium toward dimerization in the presence of disaccharide (data not shown). After this is observed, a series of ^{1}H-^{15}N HSQC spectra was acquired on RANTES at various dilutions from 1.2 to 0.025 mM protein to determine the dimer K_d of RANTES in the absence of disaccharide I-P. The relative intensities of select pairs of easily identifiable, resolved monomer and dimer resonances were monitored throughout this serial dilution, namely, H23, K25, T30, and S64. As with the MIP-1β variants, Θ_d values were plotted versus C_o for these residues in RANTES and the data were fit to eq 2b. Parts A−D of Figure 5 show the curves obtained for each of the residues. The dimer K_d values found for the separate residues were then averaged, yielding an overall dimer K_d of 34 ± 12 μM (Table 1). This average dimer K_d was found to be largely consistent to those reported previously at the higher temperature of 35 °C, in which the K_d of RANTES was shown to vary with pH from 35 to 105 μM (*27*). Because, in general, it is not feasible to obtain high-quality ^{1}H-^{15}N HSQC data at concentrations lower than about 0.020 mM, a full curve was not possible for RANTES in the presence of heparin disaccharide I-P. To estimate the increase in dimerization affinity suggested by the preliminary disaccharide experiments with RANTES, ^{1}H-^{15}N HSQC spectra were acquired on samples of 0.018 and 0.040 mM RANTES in the presence of 0.5 mM disaccharide I-P. For each of these protein concentrations, an approximate dimer K_d value was obtained in the following manner. First, the intensities of the monomer and dimer peaks for various residues (H23, K25, T30, and S64) were used in eq 3 to calculate a Θ_d value for each residue. These Θ_d values were in turn used in eq 1 to estimate a dimer K_d value in the presence of I-P for each residue. After the values calculated for each of the selected residues were averaged at 0.018 mM RANTES, an approximate dimer K_d of 4.2 μM was determined with a standard deviation of 1.4 μM (Table 1). This was in close agreement with the average K_d value determined at 0.040 mM RANTES of 5.0 μM having a standard deviation of 1.2 μM (Table 1). Together, these findings suggest that the dimerization affinity of RANTES in the presence of disaccharide is over 6-fold tighter than in the absence of disaccharide.

DISCUSSION

While several studies have shown that monomeric variants of CC and CXC chemokines can bind chemokine receptors (*31*−*33*), recent results suggest a role for the chemokine dimer in biological function that is related to the binding by

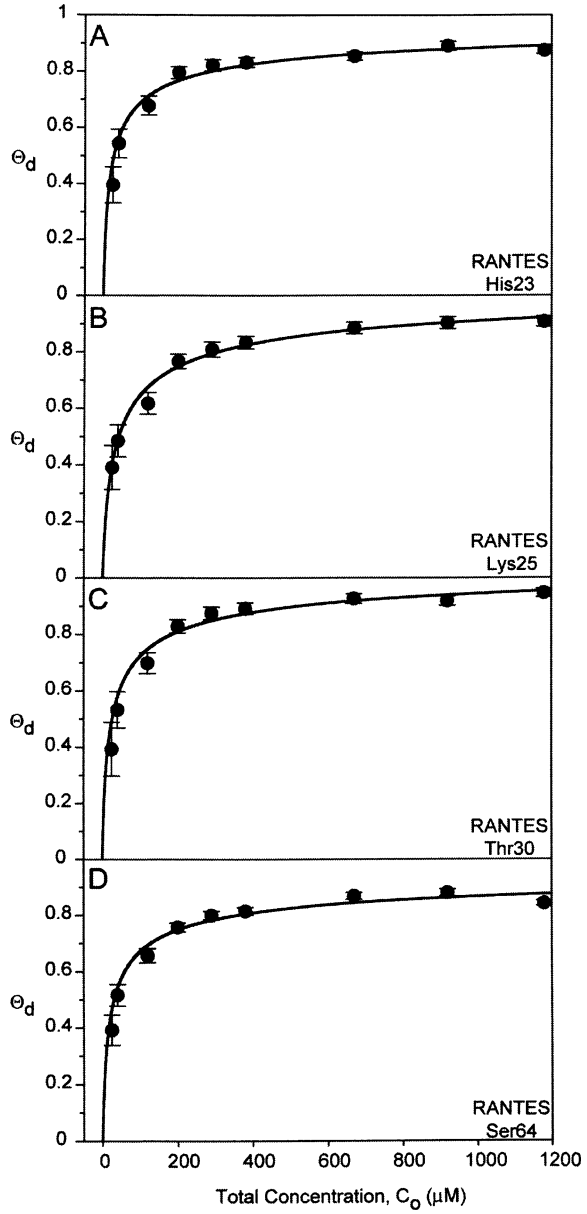

FIGURE 5: Plots of the fractional population of RANTES polypeptide subunits in the dimeric state as a function of the total concentration of subunits. Data for residues His23 (A), Lys25 (B), Thr30 (C), and Ser64 (D) are shown. The data are fit to eq 2b, yielding a dimer dissociation constant K_d. The noise level of each HSQC spectrum is used to calculate the error in Θ_d at each corresponding data point. The resulting error values are shown in the figures and are used in the weighting of each point in the curve fit.

chemokines of glycosaminoglycans. Indeed, it has been shown that both the ability to interact with GAGs and the ability to form dimers are important for the in vivo function of several chemokines, including MIP-1β (*6*). Previously, we delineated the GAG binding site on the chemokine MIP-1β and showed the participation of several N-terminal residues across the dimer interface in forming the GAG binding pocket. In addition, we showed that the GAG binding affinity for the wild type MIP-1β dimer is higher than for monomeric variants (*10*). This led to our current hypothesis that GAG binding increases the dimer affinity of MIP-1β. A quantitation of change in dimer affinity upon GAG binding has not been carried out for any chemokine, although others have investigated several aspects of chemokine oligomerization. For example, several chemokines have been reported to oligomerize in the presence of GAGs (*24*). The CXC chemokine IL-8 has been reported to bind more tightly to GAGs at lower protein concentrations, leading those authors to conclude that the IL-8 monomer binds GAGs more tightly than the dimer (*46*). However, both isothermal titration calorimetry and heparin affinity chromatography with monomeric variants of IL-8 show weaker binding to GAGs than the wild type dimer (*23*, *47*). The stoichiometry of GAG binding in the work of Kuschert and co-workers (*23*) suggested the possibility of dimerization of the IL-8 variant upon GAG binding, but previous studies by these authors indicated the monomeric variant did not dimerize in the presence of GAGs (*24*). For CC chemokines, chromatography on both MIP-1β and MIP-1α has shown that the dimeric form of each binds GAGs more tightly than monomeric variants (*8*, *13*), although earlier work concluded that the oligomerization state of MIP-1α did not affect GAG binding (*48*). Finally, surface plasmon resonance of a monomeric variant of RANTES reveals complex kinetics consistent with dimerization of the chemokine upon GAG binding (*49*).

Our results show that MIP-1β does clearly dimerize more tightly in the presence of heparin disaccharide, supporting our earlier observation that the GAG binding site for this chemokine is composed of residues from both subunits of the chemokine dimer (*10*). A variety of data support the assertion that the acidic conditions used in our NMR experiments are likely to accurately portray events occurring in the physiological pH range. Our previous work showed that both the wild type protein under acidic conditions and a nonaggregating variant at pH 6 have the same GAG binding pocket (*10*). More importantly, mutations to the NMR-revealed GAG binding site of MIP-1β were shown to have the predicted loss of activity in vivo (*6*). Our present results also demonstrate that the dimerization observed in the presence of GAGs is spectroscopically identical to that of the dimeric form of MIP-1β found in past structural studies (*26*). This finding confirms the relevance of the dimer interface found in general for CC chemokines and suggests the likelihood that GAG mediated oligomerization has the chemokine dimer as its basic unit.

The quantitative work reported here was carried out using dimer-impaired variants of MIP-1β because under most NMR-amenable conditions the dimeric form of the wild type protein greatly predominates; therefore, monomeric resonances are not visible in NMR spectra. For our experiments, the MIP-1β dimer was weakened by mutation at two separate residues, Phe13 and Leu34, both distal from each other in the monomer (Cα−Cα distance = 14 Å) and distant from the GAG binding site (distance to R46 Cα > 21 Å, Figure 1A). Mutation at each location produced folded MIP-1β variants, having spectra showing peaks from both the dimeric and monomeric forms. Each of these MIP-1β variants shows a greater than 9-fold tighter dimer in the presence of the heparin disaccharide I-P (Figure 3 and Figure 4; Table 1). In addition, under conditions where wild type RANTES, another CC chemokine, is observed as a mixture of dimer and monomer, this protein also reveals significantly tighter dimerization in the presence of disaccharide (Figure 5 and Table 1). These results suggest that the GAG binding site of RANTES may also encompass residues from both subunits

of the dimer, consistent with NMR data obtained by Proudfoot and co-workers (*14*).

It is possible that our results with disaccharides may underestimate a much larger effect on dimerization and quaternary structure that would be mediated by the longer sugars found in vivo. The optimal polysaccharide length for binding to MIP-1β is not known, but work with similar chemokines suggests longer saccharides bind more tightly (*23*). Although our studies indicate that disaccharides bind in a site that includes both subunits of the chemokine dimer and promote dimerization, the small size of the disaccharide may not allow for the full range of interactions seen for larger sugars. Longer polysaccharides cause visible aggregation in MIP-1β and other proteins, precluding their use in many types of experiments. However, longer sugars may be more likely to cause dimerization and functional oligomerization of chemokines by interacting with multiple chemokines or by simultaneously binding both GAG binding pockets of the dimer.

One unexplained aspect of our work is the apparent inability of fully monomeric MIP-1β variants to dimerize in the presence of disaccharides. Both the truncation mutant MIP(9) and the MIP-1β P8A variant are fully monomeric (*31*) and show no NMR resonances consistent with a dimer in the presence or absence of a variety of GAG disaccharides (*10*). These results are consistent with work on monomeric IL-8 and RANTES variants (*6*, *24*) but are at odds with plasmon resonance studies with truncated RANTES (*49*). However, our results are consistent with data showing that several monomeric variants (including those of MIP-1β) do not recruit cells in vivo (*6*), suggesting that dimerization even under physiological conditions is very low for these proteins.

Implications for Chemotaxis. Evidence showing that both GAG binding and dimerization are necessary for the in vivo function of several chemokines including MIP-1β underscores the probable interrelationship of GAG binding and chemokine quaternary structure (*6*). Indeed, recent cellular assays on oligomerization-impaired mutants of RANTES indicate differences in the level of oligomerization necessary for this protein to carry out various aspects of chemotaxis, including cell arrest and leukocyte spreading (*50*).

Given the available evidence, a picture of the GAG-CC chemokine structure−function relationship at a biophysical level, while not entirely clear, can be summarized as follows. Chemokines are immobilized on the endothelial surface or matrix by interacting with GAGs, which are able to manipulate the quaternary structure of the chemokine both by tightening the dimer (present work) and by facilitating oligomerization (*24*). This immobilization of chemokines is believed to be the basis of the establishment of a chemokine gradient. Chemotaxis of leukocytes occurs by movement up this chemokine concentration gradient, and therefore, one outstanding question is how the leukocytes actually use the GAG-immobilized chemokines to "sense" the changes in chemokine concentration. Receptors responsible for chemotaxis, including chemokine receptors, remain essentially evenly spaced on the surface of the cells, and the direction of the cell movement is determined by receptor occupancy by the (chemokine) ligand and by intracellular clustering of other downstream factors (*51*). The manner of presentation of increasing chemokine concentration by GAGs to leukocytes probably involves the transfer of the chemokine, possibly in various oligomeric forms, to the leukocyte surface prior to receptor binding. A ternary GAG−chemokine−receptor complex is less likely because GAGs have been shown to compete with receptors for CC chemokine binding (*8*, *15*, *52*). Therefore, chemokine concentration gradients may arise because of the local release of higher levels of chemokine from cell surface GAGs, which have "stored" the chemokines as oligomers. It is unknown whether the chemokine receptor is able to bind various quaternary forms of the chemokine, but monomeric variants of chemokines are fully functional on chemokine receptors (*31*−*33*), suggesting that dimeric and oligomeric chemokines may dissociate into monomers prior to binding the receptor.

CONCLUSION

The present results show that the dimers of MIP-1β and RANTES are tightened considerably upon binding heparin disaccharide, which is used here as a proxy for cell surface sugars. This provides insight into the specific role played by protein quaternary structure in the biological function of chemokines. In addition, the data lend quantitative evidence to a model of chemotaxis in which the chemokine concentration gradients used to mediate leukocyte movement are due to manipulation of chemokine quaternary structure by GAGs.

ACKNOWLEDGMENT

We gratefully acknowledge Karl Koshlap, Ioannis Vakonakis, and the reviewers of this paper for technical assistance. We also thank Borries Demeler for assistance with analytical ultracentrifugation. The NMR instrumentation in the Biomolecular NMR Laboratory at Texas A&M University was supported by a grant from the National Science Foundation (DBI-9970232) and the Texas A&M University System. We acknowledge the Protein Chemistry Lab and the Gene Technology Lab at Texas A&M University for their assistance. The following reagents were obtained through the NIH AIDS Research and Reference Reagent Program, Division of AIDS, NIAID, NIH: the expression vectors pET32a/Rhesus RANTES and pET32a/Rhesus MIP-1α from Dr. Francois Villinger and Dr. Aftab Ansari.

REFERENCES

1. Fernandez, E. J., and Lolis, E. (2002) Structure, function, and inhibition of chemokines, *Annu. Rev. Pharmacol. Toxicol. 42*, 469−499.
2. Mellado, M., Rodríguez-Frade, J. M., Mañes, S., and Martínez, A. C. (2001) Chemokine signaling and functional responses: The role of receptor dimerization and TK pathway activation, *Annu. Rev. Immunol. 19*, 397−421.
3. Tanaka, Y., Adams, D. H., Hubscher, S., Hirano, H., Siebenlist, U., and Shaw, S. (1993) T-cell adhesion induced by proteoglycan-immobilized cytokine MIP-1β, *Nature 361*, 79−82.
4. Springer, T. A. (1994) Traffic signals for lymphocyte recirculation and leukocyte emigration: The multistep paradigm, *Cell 76*, 301−314.
5. Weber, K. S., von Hundelshausen, P., Clark-Lewis, I., Weber, P. C., and Weber, C. (1999) Differential immobilization and hierarchical involvement of chemokines in monocyte arrest and transmigration on inflamed endothelium in shear flow, *Eur. J. Immunol. 29*, 700−712.
6. Proudfoot, A. E. I., Handel, T. M., Johnson, Z., Lau, E. K., LiWang, P., Clark-Lewis, I., Borlat, F., Wells, T. N. C., and Kosco-Vilbois, M. H. (2003) Glycosaminoglycan binding and oligomerization are essential for the in vivo activity of certain chemokines, *Proc. Natl. Acad. Sci. U.S.A. 100*, 1885−1890.

7. Peterson, F. C., Elgin, E. S., Nelson, T. J., Zhang, F., Hoeger, T. J., Linhardt, R. J., and Volkman, B. F. (2004) Identification and characterization of a glycosaminoglycan recognition element of the C chemokine lymphotactin, *J. Biol. Chem. 279*, 12598−12604.
8. Laurence, J. S., Blanpain, C., De Leener, A., Parmentier, M., and LiWang, P. J. (2001) Importance of basic residues and quaternary structure in the function of MIP-1β: CCR5 binding and cell surface sugar interactions, *Biochemistry 40*, 4990−4999.
9. Koopmann, W., Ediriwickrema, C., and Krangel, M. S. (1999) Structure and function of the glycosaminoglycan binding site of chemokine macrophage-inflammatory protein-1β, *J. Immunol. 163*, 2120−2127.
10. McCornack, M. A., Cassidy, C. K., and LiWang, P. J. (2003) The binding surface and affinity of monomeric and dimeric chemokine macrophage inflammatory protein 1β for various glycosaminoglycan disaccharides, *J. Biol. Chem. 278*, 1946−1956.
11. Graham, G. J., Wilkinson, P. C., Nibbs, R. J. B., Lowe, S., Kolset, S. O., Parker, A., Freshney, M. G., Tsang, M. L.-S., and Pragnell, I. B. (1996) Uncoupling stem cell inhibition from monocyte chemoattraction in MIP-1α by mutagenesis of the proteoglycan binding site, *EMBO J. 15*, 6506−6515.
12. Koopmann, W., and Krangel, M. S. (1997) Identification of a glycosaminoglycan-binding site in chemokine macrophage inflammatory protein-1α, *J. Biol. Chem. 272*, 10103−10109.
13. Stringer, S. E., Forster, M. J., Mulloy, B., Bishop, C. R., Graham, G. J., and Gallagher, J. T. (2002) Characterization of the binding site on heparan sulfate for macrophage inflammatory protein 1α, *Blood 100*, 1543−1550.
14. Proudfoot, A. E. I., Fritchley, S., Borlat, F., Shaw, J. P., Vilbois, F., Zwahlen, C., Trkola, A., Marchant, D., Clapham, P. R., and Wells, T. N. C. (2001) The BBXB motif of RANTES is the principal site for heparin binding and controls receptor selectivity, *J. Biol. Chem. 276*, 10620−10626.
15. Martin, L., Blanpain, C., Garnier, P., Wittamer, V., Parmentier, M., and Vita, C. (2001) Structural and functional analysis of the RANTES−glycosaminoglycans interactions, *Biochemistry 40*, 6303−6318.
16. Ali, S., Fritchley, S. J., Chaffey, B. T., and Kirby, J. A. (2002) Contribution of the putative heparan sulfate-binding motif BBXB of RANTES to transendothelial migration, *Glycobiology 12*, 535−543.
17. Chakravarty, L., Rogers, L., Quach, T., Breckenridge, S., and Kolattukudy, P. E. (1998) Lysine 58 and histidine 66 at the C-terminal α-helix of monocyte chemoattractant protein-1 are essential for glycosaminoglycan binding, *J. Biol. Chem. 273*, 29641−29647.
18. Kuschert, G. S. V., Hoogewerf, A. J., Proudfoot, A. E. I., Chung, C.-w., Cooke, R. M., Hubbard, R. E., Wells, T. N. C., and Sanderson, P. N. (1998) Identification of a glycosaminoglycan binding surface on human interleukin-8, *Biochemistry 37*, 11193−11201.
19. Mayo, K. H., Ilyina, E., Roongta, V., Dundas, M., Joseph, J., Lai, C. K., Maione, T., and Daly, T. (1995) Heparin binding to platelet factor-4, *Biochem. J. 312*, 357−365.
20. Sadir, R., Baleux, F., Grosdidier, A., Imberty, A., and Lortat-Jacob, H. (2001) Characterization of the stromal cell-derived factor-1α-heparin complex, *J. Biol. Chem. 276*, 8288−8296.
21. Amara, A., Lorthioir, O., Valenzuela, A., Magerus, A., Thelen, M., Montes, M., Virelizier, J. L., Delepierre, M., Baleux, F., Lortat-Jacob, H., and Arenzana-Seisdedos, F. (1999) Stromal cell-derived factor-1α associates with heparan sulfates through the first β-strand of the chemokine, *J. Biol. Chem. 274*, 23916−23925.
22. Campanella, G. S. V., Lee, E. M. J., Sun, J., and Luster, A. D. (2003) CXCR3 and heparin binding sites of the chemokine IP-10 (CXCL10), *J. Biol. Chem. 278*, 17066−17074.
23. Kuschert, G. S. V., Coulin, F., Power, C. A., Proudfoot, A. E. I., Hubbard, R. E., Hoogewerf, A. J., and Wells, T. N. C. (1999) Glycosaminoglycans interact selectively with chemokines and modulate receptor binding and cellular responses, *Biochemistry 38*, 12959−12968.
24. Hoogewerf, A. J., Kuschert, G. S. V., Proudfoot, A. E. I., Borlat, F., Clark-Lewis, I., Power, C. A., and Wells, T. N. C. (1997) Glycosaminoglycans mediate cell surface oligomerization of chemokines, *Biochemistry 36*, 13570−13578.
25. Stura, E. A., Martin, L., Lortat-Jacob, H., Vivès, R., and Vita, C. (2002) Heparin-aggregated RANTES can be crystallised, *Acta Crystallogr., Sect. D 58*, 1670−1673.
26. Lodi, P. J., Garrett, D. S., Kuszewski, J., Tsang, M. L.-S., Weatherbee, J. A., Leonard, W. J., Gronenborn, A. M., and Clore, G. M. (1994) High-resolution solution structure of the β chemokine hMIP-1β by multidimensional NMR, *Science 263*, 1762−1767.
27. Skelton, N. J., Aspiras, F., Ogez, J., and Schall, T. J. (1995) Proton NMR assignments and solution conformation of RANTES, a chemokine of the C-C type, *Biochemistry 34*, 5329−5342.
28. Czaplewski, L. G., McKeating, J., Craven, C. J., Higgins, L. D., Appay, V., Brown, A., Dudgeon, T., Howard, L. A., Meyers, T., Owen, J., Palan, S. R., Tan, P., Wilson, G., Woods, N. R., Heyworth, C. M., Lord, B. I., Brotherton, D., Christison, R., Craig, S., Cribbes, S., Edwards, R. M., Evans, S. J., Gilbert, R., Morgan, P., Randle, E., Schofield, N., Varley, P. G., Fisher, J., Waltho, J. P., and Hunter, M. G. (1999) Identification of amino acid residues critical for aggregation of human CC chemokines macrophage inflammatory protein (MIP)-1α, MIP-1β, and RANTES, *J. Biol. Chem. 274*, 16077−16084.
29. Graham, G. J., MacKenzie, J., Lowe, S., Tsang, L.-S., Weatherbee, J. A., Issacson, A., Medicherla, J., Fang, F., Wilkinson, P. C., and Pragnell, I. B. (1994) Aggregation of the chemokine MIP-1α is a dynamic and reversible phenomenon, *J. Biol. Chem. 269*, 4974−4978.
30. Chung, C., Cooke, R. M., Proudfoot, A. E. I., and Wells, T. N. C. (1995) The three-dimensional solution structure of RANTES, *Biochemistry 34*, 3907−9314.
31. Laurence, J. S., Blanpain, C., Burgner, J. W., Parmentier, M., and LiWang, P. J. (2000) CC chemokine MIP-1β can function as a monomer and depends on Phe13 for receptor binding, *Biochemistry 39*, 3401−3409.
32. Paavola, C. D., Hemmerich, S., Grunberger, D., Polsky, I., Bloom, A., Freedman, R., Mulkins, M., Bhakta, S., McCarley, D., Wiesent, L., Wong, B., Jarnagin, K., and Handel, T. M. (1998) Monomeric monocyte chemoattractant protein-1 (MCP-1) binds and activates the MCP-1 receptor CCR2B, *J. Biol. Chem. 273*, 33157−33165.
33. Rajarathnam, K., Sykes, B. D., Kay, C. M., Dewald, B., Geiser, T., Baggiolini, M., and Clark-Lewis, I. (1994) Neutrophil activation by monomeric interleukin-8, *Science 264*, 90−92.
34. Laurence, J. S., LiWang, A. C., and LiWang, P. J. (1998) Effect of N-terminal truncation and solution conditions on chemokine dimer stability: Nuclear magnetic resonance structural analysis of macrophage inflammatory protein 1β mutants, *Biochemistry 37*, 9346−9354.
35. Gasteiger, E., Gattiker, A., Hoogland, C., Ivanyi, I., Appel, R. D., and Bairoch, A. (2003) ExPASy: The proteomics server for in-depth protein knowledge and analysis, *Nucleic Acids Res. 31*, 3784−3788.
36. Demeler, B. (2002) Ultrascan version 6.0, A comprehensive data analysis software package for analytical ultracentrifugation experiments, University of Texas Health Science Center at San Antonio, San Antonio, Texas (http://www.ultrascan.uthscsa.edu).
37. Delaglio, F., Grzesiek, S., Vuister, G. W., Zhu, G., Pfeifer, J., and Bax, A. (1995) NMRPipe: A multidimensional spectral processing system based on UNIX pipes, *J. Biomol. NMR 6*, 277−293.
38. Garrett, D. S., Powers, R., Gronenborn, A. M., and Clore, G. M. (1991) A common sense approach to peak picking in two-, three-, and four-dimensional spectra using automatic computer analysis of contour diagrams, *J. Magn. Reson. 95*, 214−220.
39. Wishart, D. S., Bigam, C. G., Yao, J., Abildgaard, F., Dyson, H. J., Oldfield, E., Markley, J. L., and Sykes, B. D. (1995) ^{1}H, ^{13}C, ^{15}N chemical shift referencing in biomolecular NMR, *J. Biomol. NMR 6*, 135−140.
40. Vuister, G. W., and Bax, A. (1993) Quantitative J correlation: A new approach for measuring homonuclear three-bond J($H^{N}H^{\alpha}$) coupling constants in ^{15}N-enriched proteins, *J. Am. Chem. Soc. 115*, 7772−7777.
41. Levitt, M. H. (2001) *Spin Dynamics: Basics of Nuclear Magnetic Resonance*, John Wiley & Sons, New York.
42. Kim, S., Jao, S.-c., Laurence, J. S., and LiWang, P. J. (2001) Structural comparison of monomeric variants of the chemokine MIP-1β having differing ability to bind the receptor CCR5, *Biochemistry 40*, 10782−10791.
43. Taylor, J. R. (1982) in *An Introduction to Error Analysis: The Study of Uncertainties in Physical Measurements* (Commins, E. D., Ed.) pp 14−80, University Science Books, Mill Valley, CA.

44. Laue, T. M. (1995) Sedimentation equilibrium as thermodynamic tool, *Methods Enzymol. 259*, 427−452.
45. Ralston, G. (1993) *Introduction to Analytical Ultracentrifugation (Primer no. 361847)*, Beckman Instruments. Inc., Fullerton, CA.
46. Goger, B., Halden, Y., Rek, A., Mösl, R., Pye, D., Gallagher, J., and Kungl, A. J. (2002) Different affinities of glycosaminoglycan oligosaccharides for monomeric and dimeric interleukin-8: A model for chemokine regulation at inflammatory sites, *Biochemistry 41*, 1640−1646.
47. Lowman, H. B., Fairbrother, W. J., Slagle, P. H., Kabakoff, R., Liu, J., Shire, S., and Hébert, C. A. (1997) Monomeric variants of IL-8: Effects of side chain substitutions and solution conditions upon dimer formation, *Protein Sci. 6*, 598−608.
48. Ottersbach, K., and Graham, G. J. (2001) Aggregation-independent modulation of proteoglycan binding by neutralization of C-terminal acidic residues in the chemokine macrophage inflammatory protein 1α, *Biochem. J. 354*, 447−453.
49. Vivès, R. R., Sadir, R., Imberty, A., Rencurosi, A., and Lortat-Jacob, H. (2002) A kinetics and modeling study of RANTES(9−68) binding to heparin reveals a mechanism of cooperative oligomerization, *Biochemistry 41*, 14779−14789.
50. Baltus, T., Weber, K. S., Johnson, Z., Proudfoot, A. E. I., and Weber, C. (2003) Oligomerization of RANTES is required for CCR1-mediated arrest but not CCR5-mediated transmigration of leukocytes on inflamed endothelium, *Blood 102*, 1985−1988.
51. Parent, C. A., and Devreotes, P. N. (1999) A cell's sense of direction, *Science 284*, 765−770.
52. Ali, S., Palmer, A. C. V., Banerjee, B., Fritchley, S. J., and Kirby, J. A. (2000) Examination of the function of RANTES, MIP-1α, and MIP-1β following interaction with heparin-like glycosaminoglycans, *J. Biol. Chem. 275*, 11721−11727.

BI049751U